"Fission properties of actinide nuclei from proton-induced fission at 26.5 and 62.9 MeV incident proton energies"

Demetriou, P. ; Keutgen, Thomas ; Prieels, René ; El Masri, Youssef

Abstract

Fission properties of proton-induced fission on Th232, Np237, U238, Pu239, and Am241 targets, measured at the Louvain-la-Neuve cyclotron facility at proton energies of 26.5 and 62.9 MeV, are compared with the predictions of the state-of-the-art nuclear reaction code talys. The code couples the multimodal random neck-rupture model with the pre-equilibrium exciton and statistical models to predict fission fragment mass yields, pre- and post-scission neutron multiplicities, and total fission cross sections in a consistent approach. The sensitivity of the calculations to the input parameters of the code and possible improvements are discussed in detail. © 2010 The American Physical Society.

Document type : *Article de périodique (Journal article)*

Fission properties of actinide nuclei from proton-induced fission at 26.5 and 62.9 MeV incident proton energies

P. Demetriou,[1] Th. Keutgen,[2] R. Prieels,[2] and Y. El Masri[2]
[1]*Institute of Nuclear Physics, NCSR "Demokritos", GR 153 10 Athens, Greece*
[2]*FNRS and Institut de Physique Nucléaire, Université catholique de Louvain, B-1348 Louvain-la Neuve, Belgium*
(Received 28 January 2010; revised manuscript received 6 October 2010; published 12 November 2010)

Fission properties of proton-induced fission on ^{232}Th, ^{237}Np, ^{238}U, ^{239}Pu, and ^{241}Am targets, measured at the Louvain-la-Neuve cyclotron facility at proton energies of 26.5 and 62.9 MeV, are compared with the predictions of the state-of-the-art nuclear reaction code TALYS. The code couples the multimodal random neck-rupture model with the pre-equilibrium exciton and statistical models to predict fission fragment mass yields, pre- and post-scission neutron multiplicities, and total fission cross sections in a consistent approach. The sensitivity of the calculations to the input parameters of the code and possible improvements are discussed in detail.

DOI: 10.1103/PhysRevC.82.054606 PACS number(s): 25.85.Ge, 24.10.−i, 24.60.−k, 24.75.+i

I. INTRODUCTION

Nuclear fission at intermediate energies, between 10 and 200 MeV, is considered to be of importance in applications such as accelerator-driven systems (ADSs) for the transmutation of nuclear waste, the production of energy and radioisotopes. Although the exact role of intermediate-energy fission in ADSs will depend on the design of the system [1], the ability to adequately describe the process and its products is a prerequisite to any subsequent appreciation of its significance. In spite of this, intermediate-energy fission remains one of the least understood nuclear processes due to its complexity and the fact that fission is a dynamic rather than a static process. With increasing energy above a few MeV, fission is likely to compete with particle evaporation. At even higher energies, prompt emission process such as pre-equilibrium emission (PE) will also play an important role. The number of particles emitted by these processes increases with energy leading to a large number of residual nuclides with various excitation energies that can contribute to fission. Furthermore, the fission properties of all nuclides contributing to the fission reaction also vary strongly with energy. The experimental data are thus a superposition of contributions from all the different fissioning nuclei and there is no means, so far, to disentangle the individual contributions without any guidance from theory. Several attempts have been made to describe the fission properties, particularly of actinide nuclei, and how they vary with excitation energy (see Ref. [2] and references therein). Many of the models mentioned in the above reference depend on systematics in order to produce fission fragment yields at intermediate energies. However, since there are very few data on fission properties, it is very difficult to develop systematics over a wide range of mass numbers and excitation energies. Furthermore, as already mentioned, in almost all cases the measurements are a superposition of various contributing fissioning nuclides that are most likely to differ with target nucleus and incident energy. Therefore, the systematics extracted in one case may not be applicable in another different case. More fundamental approaches to the description of intermediate-energy fission have also been developed [2] and have been implemented in the state-of-the-art nuclear reaction code TALYS [3]. This code couples the nuclear reaction models (pre-equilibrium and statistical models) with the multimodal random-neck rupture model (MM-RNRM) of Refs. [2,4] to predict fission fragment mass and charge distributions. The statistical model implemented in TALYS calculates the fission cross section for each fissioning nuclide as a function of excitation energy, in competition with the other processes such as particle evaporation and PE emission and also produces total fission cross sections and pre-scission neutron multiplicities. In a second stage, the total fission-fragment mass distributions are constructed from the contributions of the different fissioning nuclides and the relative yields of the fission fragments determined in the frame of the MM-RNRM. To test the validity of this coupling method and assess the predictive power of the code, extensive comparisons with existing experimental data are necessary.

Although a large number of neutron-induced [5–8] and proton-induced [9–13] fission experiments have been carried out at energies above 10 MeV, very few of these measurements have included fission fragment mass distributions and neutron multiplicities, and even fewer coincident neutron and light charged-particle energy and angular distributions.

In Ref. [14], a complete series of measurements of fission properties, including total fission cross sections $\sigma_f^{\rm tot}$, pre- and post-scission neutron multiplicities, $\nu^{\rm pre}$ and $\nu^{\rm post}$, respectively, coincident neutron energy and angular distributions in and out of the reaction plane, as well as fission fragment FF mass distributions, was presented for the first time for proton-induced fission on the five actinide nuclei ^{232}Th, ^{237}Np, ^{238}U, ^{239}Pu, and ^{241}Am, at proton energies of 26.5 MeV and 62.9 MeV. Furthermore, $\sigma_f^{\rm tot}$, $\nu^{\rm pre}$, and $\nu^{\rm post}$ were compared with the predictions of TALYS [3] using different sets of fission barrier parameters. The comparison showed that the calculations are sensitive to the fission barriers but that none of the sets are able to adequately describe all these three observables.

In a continuation of the work of Ref. [14], we present herein a more complete investigation of the models and input parameters of TALYS by comparing the predictions of the code with all the fission properties of the five actinide nuclei ^{232}Th, ^{237}Np, ^{238}U, ^{239}Pu, and ^{241}Am, including FF mass distributions, $\sigma_f^{\rm tot}$,

ν^{pre}, and ν^{post}, measured at proton energies of 25.6 MeV and 62.9 MeV [14]. It must be pointed out that the ν^{pre} values discussed herein include neutrons emitted prior to fission by both PE and evaporation processes. In Sec. II, we briefly present the method and models incorporated in TALYS and a comparison between predictions and experiment using the optional input parameters. The two stages in the calculations leading to the fission products as already mentioned above are discussed separately. Therefore, in Sec. II A we discuss possible improvements in the calculations of the contributions of the competing channels in the first stage of the method. In Sec. II B, we present the effects of modifying the contributions of the fission modes calculated in the second stage of the method. Our conclusions are drawn in Sec. III.

II. FISSION PROPERTIES

A detailed description of the procedure followed to determine fission fragment yields in TALYS can be found in Refs. [2–4]. Here we mention some important aspects of the approach only. The pre-scission emission of light particles, by pre-equilibrium (PE) and evaporation processes, results in the creation of different residual nuclei RN at various excitation energies $E^{\star}_{\text{RN}}$. If the RN undergoes fission it will be specifically identified as a fissioning system FS with a certain probability determined by its corresponding fission cross section. The statistical model gives the fission cross section per excitation energy $E^{\star}_{\text{FS}}$ for each FS. If an RN survives fission, it continues to evaporate particles and gammas until it forms the final heavy residue with its respective cross section. In case of fission, the FF masses and charges are determined per given excitation-energy bin $E^{\star}_{\text{FS}}$ in a fissioning system characterized by (Z_{FS}, A_{FS}, $E^{\star}_{\text{FS}}$), for which the fission cross section exceeds some minimum value. For sake of simplicity, in the following we shall denote $c = (Z_{\text{FS}}, A_{\text{FS}}, E^{\star}_{\text{FS}})$. The total fragment mass distribution is given by a sum over all contributing parts c weighted by the corresponding partial fission cross section $\sigma_f(c)$:

$$\sigma(A_{\text{FF}}) = \sum_c \sigma_f(c) Y(A_{\text{FF}}; c), \tag{1}$$

where $Y(A_{\text{FF}}; c)$ is the relative yield of a fission fragment with mass A_{FF} originating from a fissioning system FS characterized by the initial condition c.

In TALYS, the partial fission cross section $\sigma_f(c)$ and total fission cross section σ_f^{tot} are calculated within the statistical model using Hill-Wheeler transmission coefficients. The relative yield [$Y(A_{\text{FF}})$] of an FF with mass A_{FF} is determined by the MM-RNRM of Brosa *et al.* [4], which was further developed by Ref. [2] to include temperature dependence (T) in the calculation of the potential energy surface (PES) of the nucleus. According to this model, the potential energy surface is calculated on the basis of the liquid drop model (LDM) with shell-model corrections (Strutinsky Integral) and T dependence. A search for the fission channels in deformation space, yields three fission modes (FMs), namely the superlong (SL), the standard I (STI), and the standard II (STII), with the respective fission barriers and pre-scission shapes as a function of T. This way, the melting of shell effects with T is naturally incorporated. The T-dependent fission barriers and pre-scission shape parameters thus obtained serve as input for the fragment mass distribution computations.

TABLE I. Experimental and calculated total fission cross sections obtained from TALYS using the fission-barrier parameters from the compilation of Maslov [17], RFRM [18], and RLDM [19].

Target	σ_f^{tot} (mb) Maslov [17]	σ_f^{tot} (mb) RFRM [18]	σ_f^{tot} (mb) RLDM [19]	σ_f^{tot} (mb) Expt.
		$E_p = 26.5$ MeV		
^{232}Th	400	1274	108	1190 ± 60
^{238}U	1171	1551	761	1540 ± 77
^{237}Np	1455	1502	97.4	1170 ± 118
^{239}Pu	1444	1583	1422	1760 ± 88
^{241}Am	1408	1574	1451	1650 ± 83
		$E_p = 62.9$ MeV		
^{232}Th	1104	1369	329	1550 ± 78
^{238}U	1157	1958	945	1980 ± 99
^{237}Np	1752	1922	308	1830 ± 184
^{239}Pu	1771	2042	1241	2320 ± 116
^{241}Am	1707	2048	1898	2150 ± 108

Thus, each relative yield $Y(A_{\text{FF}}; c)$ becomes a sum over the contributions of the three dominant FMs

$$Y(A_{\text{FF}}; c) = \sum_{\text{FM=SL,STI,STII}} W_{\text{FM}}(c) Y_{\text{FM}}(A_{\text{FF}}; c), \tag{2}$$

where $W_{\text{FM}}(c)$ is the weight of the given FM, and $Y_{\text{FM}}(A_{\text{FF}}; c)$ is the corresponding mass distribution of the FS characterized by c. The latter mass distribution per fission mode is calculated by the MM-RNRM [4]. According to the model, after the passage over the barriers, a neck starts to form. If the neck becomes flat its rupture may occur randomly anywhere. The probability of cutting the neck at an arbitrary position determines the pre-scission shape and hence the FF mass distributions. If a pre-scission shape has a very long neck, the mass distribution will be broad, whereas if it has a short neck the mass distribution will be narrow.

Total fragment mass distributions $\sigma(A_{\text{FF}})$ were calculated with TALYS with the same sets of fission barriers that were used to compare total fission cross sections σ_f^{tot} and $\nu^{\text{pre,post}}$ in [14] (see Table I for details). PE emission was calculated with the global exciton model developed by Ref. [15]. The ground-state and saddle-point nuclear level densities were obtained from the constant-temperature-Fermi-gas model parametrization of Ref. [3], obtained from global fits to all existing data on low-lying states and neutron-resonance spacings. The nucleon optical model potential of Ref. [16], a deformed phenomenological optical potential for the actinides in question at energies up to 200 MeV, was used. The resulting $\sigma(A_{\text{FF}})$ are compared with the experimental mass distributions of Ref. [14] in Figs. 1 and 2 for proton-beam energies 26.5 and 62.9 MeV, and the five actinide targets ^{232}Th, ^{238}U, ^{237}Np, ^{239}Pu, and ^{241}Am. The uncertainties in the determination of the experimental masses was estimated to be of the order of 6% [14].

As can be seen in the figures, none of the proposed fission-barrier sets is able to give a satisfactory description

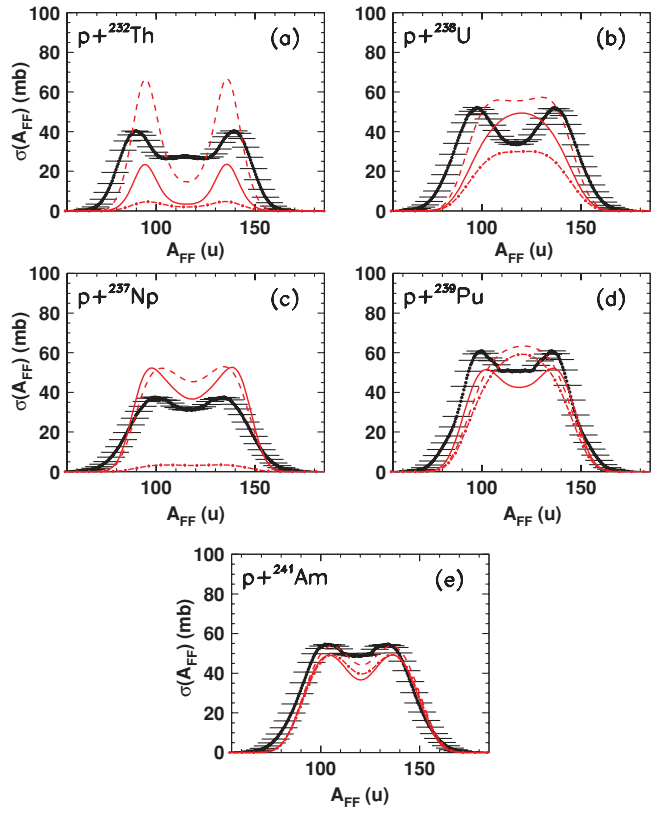

FIG. 1. (Color online) Total mass distributions $\sigma(A_{\rm FF})$ of fission fragments for proton-induced fission on ^{232}Th, ^{238}U, ^{237}Np, ^{239}Pu, and ^{241}Am measured at incident proton energy 26.5 MeV [14] (black dot symbols). Also plotted are the calculated mass distributions obtained with TALYS [3] using the fission barriers of Maslov [17] (red solid line), RFRM [18] (red dashed line), and the RLDM [19] (red dot-dashed line). The horizontal error bars here and in the following figures express the uncertainties in the experimental FF mass distributions taken to be equal to those of the symmetric mass partition [14].

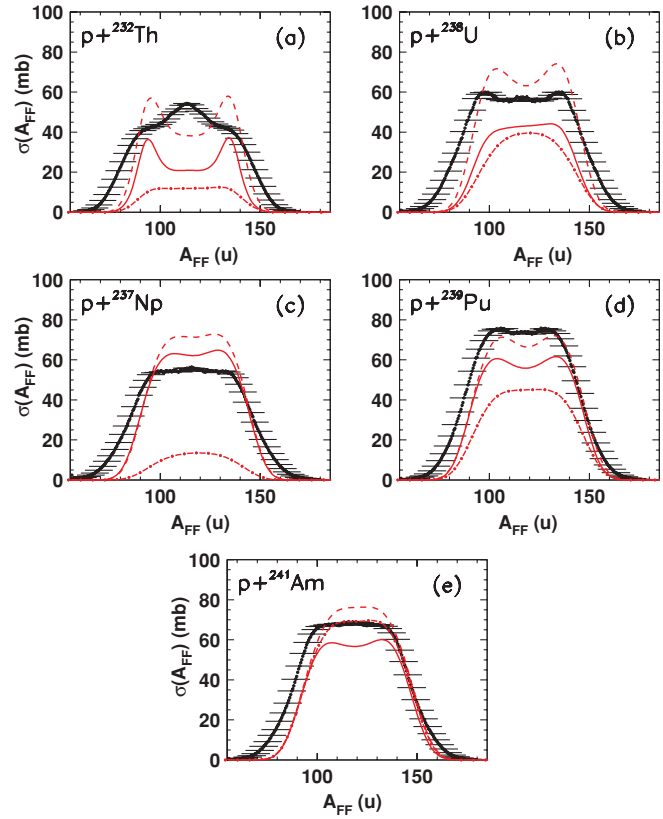

FIG. 2. (Color online) Same as Fig. 1 but at proton incident energy 62.9 MeV.

of all five actinide target nuclei. The deviations in magnitude correspond directly to the deviations in the total fission cross sections described in Ref. [14] and shown in Table I. The barriers of Maslov [17] for example, tend to underestimate the magnitude of the mass distributions of all the actinides, with the most marked underestimation being that of ^{232}Th, in direct analogy with the total fission cross sections of Table I. It is worth recalling here, particularly in view of its relevance to the discussion that follows, that although TALYS offers a choice of different sets of fission-barrier parameters for the fission cross section calculations, the fission barriers and pre-scission shapes used in the calculations of $Y_{\rm FM}(A_{\rm FF};c)$ are exclusively those obtained with the T-dependent LDM-plus-shell corrections inherent in the MM-RNRM of Ref. [2]. Consequently, the use of the fission barriers [17–19] will only affect the calculations of $\sigma_f(c)$ and not of $Y_{\rm FM}(A_{\rm FF};c)$ and will, therefore, only partly affect the total FF mass distributions $\sigma(A_{\rm FF})$ through $\sigma_f(c)$. This inconsistency in the calculations of $\sigma_f(c)$ and $Y_{\rm FM}(A_{\rm FF};c)$ is a limitation of TALYS when it comes to calculating mass distributions in the actinide mass region.

Apart from deviations in magnitude, one also observes a marked difference in the shapes of the mass distributions. In some cases, the calculated mass distributions are more symmetric at the lower incident energy of 26.5 MeV than at 62.9 MeV, as in the cases of a ^{238}U target with fission barriers of [17,18], and [19], and a ^{239}Pu target with barriers of [18,19]. This is contrary to what is generally expected from the vanishing of shell effects with increasing incident energy. In fact, asymmetric mass distributions are related to shell effects in the fission fragments, which are expected to vanish gradually with increasing excitation energies. The mass distribution for an FS should, therefore, become more symmetric with increasing bombarding energy rather than the opposite, which is observed in Figs. 1 and 2. Another case worth noting is that of ^{232}Th target with the pronounced symmetric peak at 62.9 MeV, and a much less pronounced one at 26.5 MeV. The calculations fail to reproduce this peak and, moreover, when using Maslov's and the RFRM barriers, they give an incorrect relative contribution of symmetric to asymmetric fission. Similar results were reported in Ref. [2], wherein calculations using the statistical model plus T-dependent MN-RNRM model, were compared with the much older set of data on proton-induced fission on ^{232}Th at projectile energies ranging from 13 to 53 MeV of Ref. [20]. The comparison [2] already showed that the shapes of the mass distributions at projectile energies of 13 and 20 MeV could be described reasonably well, whereas the contribution of asymmetric over symmetric

fission obtained at 53 MeV was completely wrong and could not account for the symmetric peak observed in the data.

From Eqs. (1) and (2) it follows that the FF mass distributions depend on the relative contributions of the various fissioning systems FS through $\sigma_f(c)$ and also on the relative contributions of the three fission modes, STI, STII, and SL through $W_{\rm FM}(c)$. In the following sections, we shall attempt to modify these contributions [$\sigma_f(c)$ and $W_{\rm FM}(c)$] in order to improve the description of all the experimental data of Ref. [14], including FF mass distributions $\sigma_f^{\rm tot}$ and $\nu^{\rm pre,post}$. For this purpose, we shall use as our starting point the set of experimentally extracted fission barriers of Maslov [17] where available, and where they are not available the RFRM barriers [18] which gave the best agreement with the experimental $\sigma_f^{\rm tot}$ (see Table I) in spite of the fact that they are single-humped barriers. The former barriers are preferred, although they did not give the best results in Ref. [14], as they are all double-humped barriers and are therefore in agreement with the existing experimental evidence showing that the actinides under study have double-humped fission barriers. The other input parameters remain as described at the beginning of this section.

A. Fissioning systems

1. General comparison

Each fissioning system FS with a partial fission cross section $\sigma_f(c)$ above a certain threshold contributes to the mass distribution with a weight that is determined by the corresponding fission cross section and thus constitutes a fission channel c. The shape of the mass distribution of each FS depends on the relative contributions of the various FM as outlined in Eq. (2). The shape of the total fragment mass distribution also depends on the relative contributions of the different FS. The initial compound nucleus (CN) is expected to contribute to fission at the highest excitation energies mostly, while the more depleted RN will contribute at lower excitation energies since the pre-scission (sum of PE and evaporation contributions) emitted neutrons or protons will have removed a significant part of $E^{\star}_{\rm CN}$. This is shown in Figs. 3 to 6 where the contributions of the various FS are plotted per excitation energy $E^{\star}$ for the typical actinide targets ^{232}Th and ^{238}U. The different CN and RN contributing to fission and hence constituting FS are indicated by their chemical symbol and by their mass number $A_{\rm FS}$. The contribution of CN and the less-depleted RN are shown to peak at the higher $E^{\star}$ while the more-depleted RN peak at lower $E^{\star}$. An exception to this general behavior is observed in the third panel of Fig. 6 showing the fission contributions of the residual nuclei Pa to proton-induced fission on a ^{238}U target at $E_p = 62.9$ MeV. According to the figure, the less-neutron-depleted isotopes of Pa prefer to fission at the lower excitation energies, most likely because of the strong competition with the neutron emission channel at higher excitation energies that dominates, while the more-depleted ones prefer to fission at the higher excitation energies. Note that, while the initial CN contribution is expected to appear as a single peak at the $E^{\star}_{\rm max}$,in the above-mentioned figures it shows a spread in energy, attributed to the fact that, in TALYS, the deexcitation of the initial CN by photon emission is followed right down to the ground state. Different

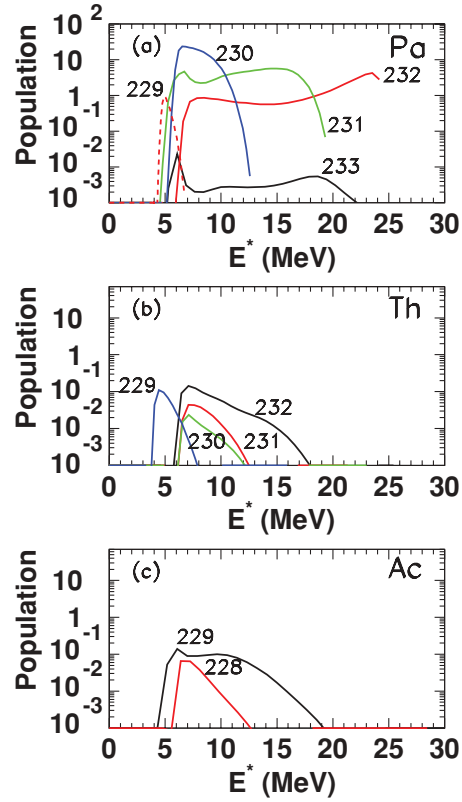

FIG. 3. (Color online) Semilogarithmic plot of the excitation-energy distribution of the fissioning systems in proton-induced fission on ^{232}Th target at incident energy of 26.5 MeV obtained with the default version of TALYS [3]. The contributing FS are denoted by their chemical symbol at the upper right corner and by their mass numbers on the corresponding curves. Please note the cut at 10^{-3} in the displayed population meaning that weaker contributions of a given nucleus do not show up and are represented by a continuous line of the same color along the $E^{\star}$ axis.

FS contribute to fission in the case of these two actinide targets leading to entirely different mass partitions. The higher the excitation energy $E^{\star}_{\rm FS}$ of FS, the more symmetric mass distribution it will yield, since shell effects tend to be washed out with increasing excitation energy. Figures 7 to 10 display the contributions of the individual FSs to the total FF mass distribution. The symmetric mass partitions generally correspond to the more excited FS such as the initial CN or at most to those RN that have been formed after the pre-scission emission of one neutron or proton. It follows that the relative contributions of symmetric and asymmetric mass partitions are strongly related to the pre-scission neutron multiplicities. The discrepancies in magnitude in the FF mass distributions are mainly a consequence of the underestimated or overestimated total fission cross sections (see Ref. [14] and Table I), since the integral of the area outlined by the FF mass distributions in the figures is related to the $\sigma_f^{\rm tot}$ of the corresponding target actinide. Similar comparisons can be made for the other three actinides but are not shown here to save space. Comparisons made in complete analogy for neutron-induced fission on the same targets and at comparable energies, would also show different FS contributing to the respective

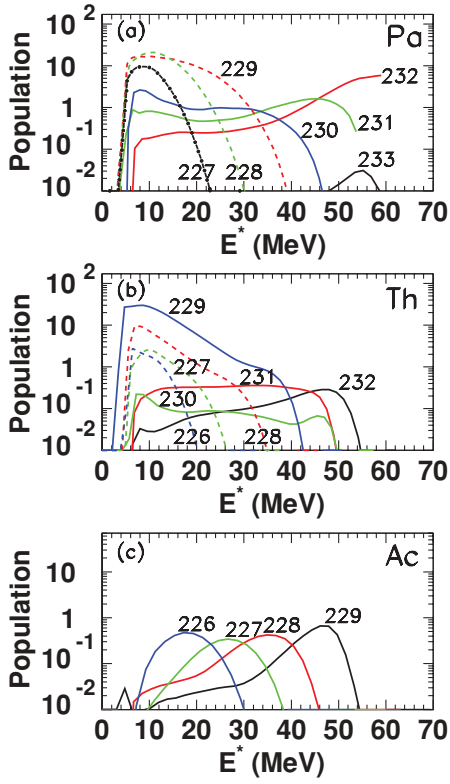

FIG. 4. (Color online) Same as in Fig. 3 (^{232}Th target) but for 62.9-MeV proton incident energy.

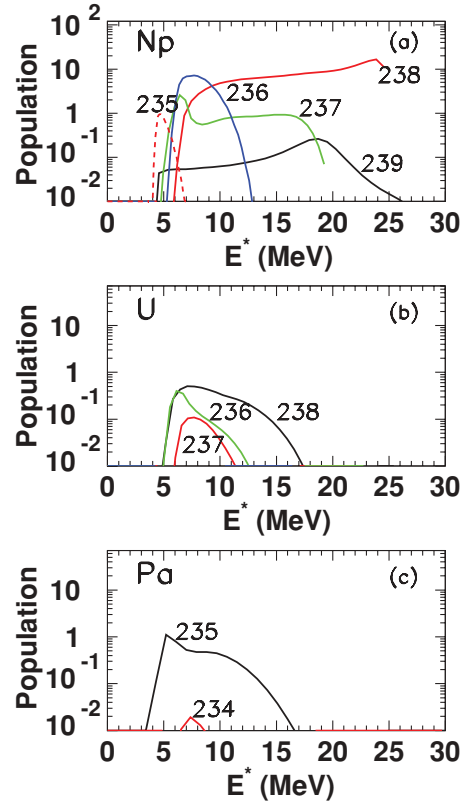

FIG. 5. (Color online) Same as in Fig. 3 but for ^{238}U target.

fission process, as well as different FF mass distributions. Neutrons incident on Th and U targets are more likely to produce FSs in the Th and U isotopic chains, respectively, through the preferred neutron decay channel, rather than the Pa and Np isotopes produced by protons incident on the same targets. The distinct nuclear properties of these neighboring actinides (i.e., deformation, shell structures, transition from symmetric to asymmetric fission, etc.) are still expected to play a role in fission at the energies between 25 and 65 MeV studied herein and, thus, will show up in the yields and shapes of the corresponding FF mass distributions. This is clearly seen in the comparison of the FF mass distribution obtained from neutron-induced fission on ^{232}Th at the incident energy of 60 MeV [8] with that obtained from proton-induced fission on the same target at $E_p = 62.9$ MeV in this work. The former FF mass distribution includes mixed contributions of symmetric and asymmetric mass partitions, while the latter (see Fig. 2) shows a pronounced symmetric peak. Therefore, one must be very careful before drawing any conclusions from the comparison between neutron- and proton-induced reactions mainly in the actinide region.

2. *Improvements in* TALYS *predictions*

In this section, we shall modify the contributions of the individual FS so as to increase $\sigma_f^{\rm tot}$ and the magnitude of the FF mass distributions, and also improve the shapes of the FF mass distributions and the pre-scission neutron multiplicities. This means that both the absolute and relative contributions $\sigma_f(c)$ of FS giving symmetric and asymmetric mass partitions will be readjusted. Finding the model parameters that will describe all the above-mentioned measured properties proves to be a challenging task as will be shown in the following.

The fission cross sections of all fissioning CN and RN are modified by adjusting (i) the strength M_2 of the matrix element of the exciton model governing PE emission [15], within the limits determined by the exciton model implemented in TALYS [3]. In a second step, the $\sigma_f(c)$ of certain FS are further modified by varying (ii) the nuclear level densities (NLDs) at the saddle points, and (iii) the fission barrier heights (B_f) of Maslov [17] that enter the Hauser-Feshbach formalism for fission cross sections, again within the allowed limits in TALYS. The above-mentioned parameters are afflicted by large uncertainties due to the lack of independent experimental data for the actinide nuclei included in this study and, therefore, they are open to some modification. In the case of (ii) in particular, it is well known that collective effects in nuclear level densities play an important role in fission. In TALYS, such effects are included explicitly by using collective enhancement factors $K_{\rm vib}(E^\star)$ and $K_{\rm rot}(E^\star)$ [17] (for vibrational and rotational, respectively) on top of the level density $\rho(E^*_{\rm FS}, J, \Pi)$ that describes purely single-particle excitations. The gradual disappearance of the collective mode $[K_{\rm rot}(E^\star)]$ with $E^\star$ is taken into account by means of an empirical damping function whose parameters are set arbitrarily. The exact formulas used to describe $K_{\rm vib}(E^\star)$ and $K_{\rm rot}(E^\star)$ can be found in Refs. [3,17]. Since not much is known experimentally about rotational excitations at the saddle-point deformations, in TALYS the

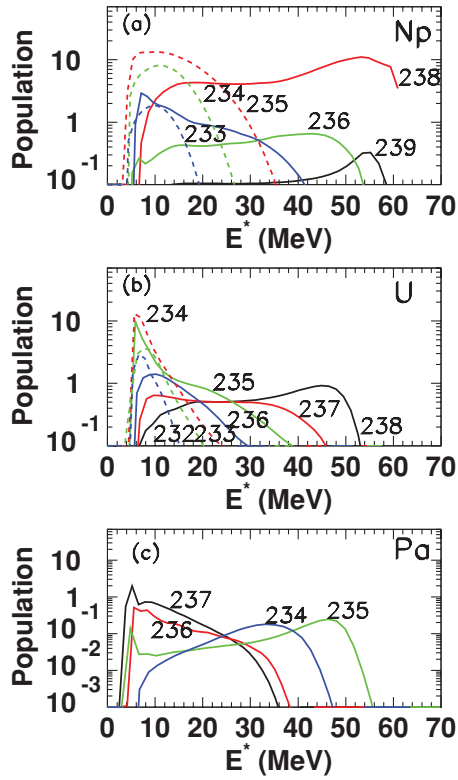

FIG. 6. (Color online) Same as in Fig. 5 but for 62.9-MeV proton incident energy.

value of $K_{\rm rot}(E^\star)$ is allowed to vary by multiplying the original formula by a multiplicative constant $K_{\rm rot}^{\rm const}$ whose values range from 0.01 to 100. The empirical damping function mentioned above and the multiplicative constant $K_{\rm rot}^{\rm const}$ are introduced so that $K_{\rm rot}(E^\star)$ gradually diminishes with increasing $E^\star$ to a minimum value of 1. The latter minimum value implies that

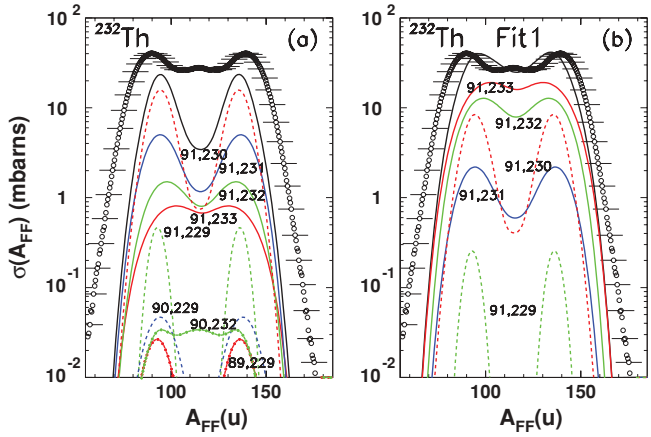

FIG. 7. (Color online) (a) Fission fragment mass distributions for proton-induced fission on ^{232}Th at incident energy of 26.5 MeV (open black circles). Left: Also plotted are the calculated total mass distributions (full black line) and the contributions of the individual FS with $Z_{\rm FS} = 91$, 90 and their corresponding initial mass values $A_{\rm FS}$ (colored lines) obtained with TALYS [3] using the default values of B_f [17] and $K_{\rm rot}$ parameter. (b) Same as in (a) but with modified calculated mass distributions from Fit 1 (see text for details).

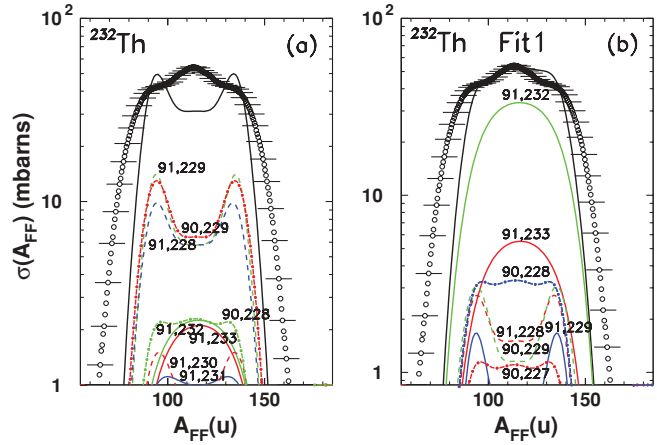

FIG. 8. (Color online) Same as in Fig. 7 but for 62.9-MeV proton incident energy.

shell effects and, hence, collective effects have been washed out at the given $E^\star$. The strength M_2 of the exciton model, on the other hand, determines how much of the initial incident flux is emitted as PE emission and how much is damped into the next more complex and excited stage of the reaction that may lead to fission. The allowed values of M_2 range from 0.1 to 10. The height of the fission barrier B_f can take any reasonable value.

The results of the modified FS contributions are shown in the right-hand sides of Figs. 7 and 8 for ^{232}Th and ^{238}U under the label "Fit 1." From the results it is clear that, overall, larger values of M_2 favor damping of the PE strength to more complex excited states that eventually lead to fission. Lower values of M_2 favor PE emission over evaporation, leaving the RN with much less excitation energy, especially at low incident energies such as $E_p = 26.5$ MeV. In this case, one obtains lower values of $\sigma_f^{\rm tot}$ and $\nu^{\rm pre}$ since there is only enough available excitation energy to emit one PE particle prior to fission. Further improvement is possible by varying the $K_{\rm rot}^{\rm const}$ and B_f of some of the individual FS. The search for the best combined values of M_2, $K_{\rm rot}^{\rm const}$, and B_f does not necessarily lead to a unique set. Different combinations of these three parameters for different FS may lead to similar

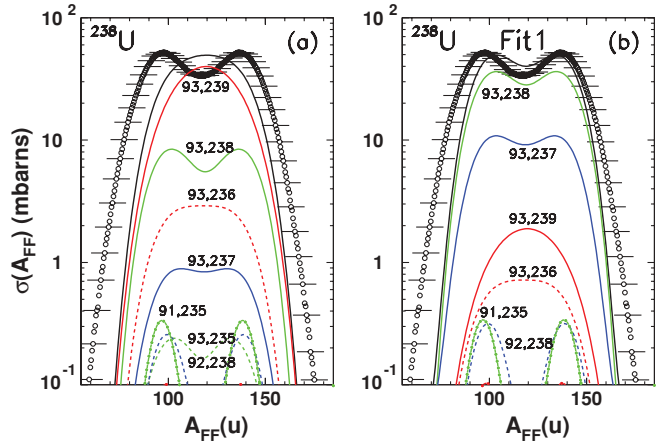

FIG. 9. (Color online) Same as in Fig. 7 but for ^{238}U target.

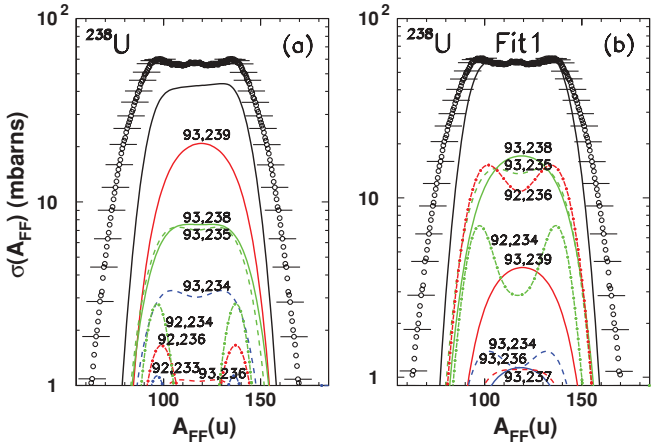

FIG. 10. (Color online) Same as in Fig. 9 (^{238}U target) but for 62.9-MeV proton incident energy.

or even better results. Our search showed that, in nearly all of the cases studied, obtaining the desired effect required drastic adjustments of some of the individual $\sigma_f(c)$ (i.e., by setting $K_{\rm rot}^{\rm const} = 100$ or 0.01). The final values of the adjusted parameters are shown in Table II. Only those FS whose $K_{\rm rot}^{\rm const}$ and B_f were actually modified are displayed in the table. The resulting $\sigma_f^{\rm tot}$ and $\nu^{\rm pre,post}$ are compared with the experimental data [14] in Table III.

The FF mass distributions obtained as a result of the modifications of Table II are shown in Figs. 11 and 12 (Fit 1) for the actinide targets studied. As can be seen from these figures, the magnitude of the mass yields is significantly improved for all the target nuclei. In the case of ^{232}Th, ^{239}Pu, and ^{241}Am targets at $E_p = 26.5$ MeV, M_2 is increased from the default value $M_2 = 0.8$ to $M_2 = 2$, thus leading to a reduction of PE emission and an enhancement of the CN decays and fission contributions. However, the increase in M_2 is not sufficient to produce the desired agreement with data. For ^{232}Th targets, for example, the CN and one subsequent RN are also enhanced in order to enhance symmetric fission contributions to the total mass distribution. The latter adjustment also results in a lower value of $\nu^{\rm pre}$ as shown in Table III. On the other hand, the contributions of several more neutron-depleted RN are enhanced for ^{239}Pu and ^{241}Am targets in order to increase the contribution of asymmetric fission with respect to symmetric fission. At the same time, the relative contributions of these RN also lead to slightly lower values of $\nu^{\rm pre}$ for ^{239}Pu and ^{241}Am targets, which agree with the experimental ones within the error bars (see Table III). In the case of a ^{238}U target, an increase in M_2 led to more symmetric mass distributions than needed, therefore M_2 is decreased to 0.6 to get a more asymmetric shape. The enhancement of the asymmetric contribution to $\sigma(A_{\rm FF})$ and $\nu^{\rm pre}$ is also achieved by reducing the contribution of the initial excited CN and increasing those of the subsequent neutron-depleted RN. For ^{237}Np at $E_p = 26.5$ MeV, PE emission is enhanced ($M_2 = 0.2$) in order to reduce the $\sigma_f^{\rm tot}$ and the magnitude of the mass distribution that overestimated the experimental data. To reduce $\nu^{\rm pre}$, the $K_{\rm rot}^{\rm const}$ parameter of the first CN had to be increased while those of the subsequent RN were reduced. The contribution of ^{237}Np also had to be

TABLE II. Best values of M_2, $K_{\rm rot}^{\rm const}$, and B_f according to Fit 1 as discussed in the text. Only those FS whose $K_{\rm rot}^{\rm const}$ were actually adjusted are shown. Modified (and original) values of B_f [17] are displayed only in cases where the B_f values were actually modified.

Target	M_2	$A_{\rm FS}$	$K_{\rm rot}^{\rm const}$	$B_f^{\rm in}$ (MeV)	$B_f^{\rm out}$ (MeV)
		$E_p = 26.5$ MeV			
^{232}Th	2	^{233}Pa	30		
		^{232}Pa	25		
^{238}U	0.6	^{239}Np	0.01		
		^{238}Np	5		
		^{237}Np	100		
^{237}Np	0.4	^{238}Pu	10		
		^{236}Pu	0.5	5.9 (3.6)	
		^{235}Pu	0.5	5.9 (3.4)	
		^{237}Np	100		
^{239}Pu	2	^{239}Am	5		
		^{238}Am	100	3 (5)	
		^{239}Pu	100		
		^{238}Pu	10		
^{241}Am	2	^{242}Cm	0.2		
		^{241}Cm	100	6 (7.15)	4.5 (5.5)
		^{240}Cm	100		
		^{239}Cm	100		
		^{241}Am	100	5 (6)	4.3 (5.35)
		$E_p = 62.9$ MeV			
^{232}Th	3	^{232}Pa	25.		
		^{231}Pa	0.1		
		^{229}Pa	0.1		
		^{228}Pa	0.1		
		^{229}Th	0.1		
^{238}U	2	^{239}Np	0.01		
		^{235}Np	10		
		^{236}U	50		
		^{234}U	50		
^{237}Np	0.4	^{237}Pu	10		
		^{236}Pu	0.5	5.9 (3.6)	
^{239}Pu	3	^{240}Am	0.1		
		^{236}Am	100		
		^{238}Pu	10		
		^{237}Pu	10		
^{241}Am	1.5	^{242}Cm	0.2		
		^{239}Am	5		

increased substantially. On the whole, from the comparison of $\sigma_f^{\rm tot}$ and $\nu^{\rm pre,post}$ with the measured values [14] shown in Table III, one sees that at $E_p = 26.5$ MeV, the values of $\nu^{\rm pre}$ of Fit 1 are more or less in agreement with the data within the experimental uncertainties. The values of $\nu^{\rm post}$, however, remain higher than the experimental ones for all target actinides. A similar trend is seen in the default values of $\nu^{\rm post}$ and may be attributed to the rather simple approach that is used to estimate $\nu^{\rm post}$ in TALYS [4]. According to the latter approach, the total excitation energy of the primary FF is released through post-scission neutron and γ-ray emissions. The kinetic energy of the emitted neutrons is taken to be 3/2 times the fragment temperature while the total energy carried off by the γ ray is taken to be half the separation

TABLE III. Total fission cross sections $\sigma_f^{\rm tot}$, pre- and post-scission neutron multiplicities obtained from TALYS using Fit 1 input parameters (see Table II) compared with experimental data [14].

Target	Fit 1			Experiment [14]	
	$\sigma_f^{\rm tot}$ (mb)	$\nu^{\rm pre}$	$\nu^{\rm post}$	$\nu^{\rm pre}$	$\nu^{\rm post}$
		$E_p = 26.5$ MeV			
^{232}Th	1041	0.77	4.40	0.93 ± 0.44	2.88 ± 0.29
^{238}U	1361	1.22	4.50	1.49 ± 0.70	3.31 ± 0.31
^{237}Np	1013	0.97	4.46	0.85 ± 0.51	3.79 ± 0.25
^{239}Pu	1567	1.40	4.53	1.16 ± 0.59	4.16 ± 0.26
^{241}Am	1558	0.94	5.09	1.03 ± 0.24	4.26 ± 0.12
		$E_p = 62.9$ MeV			
^{232}Th	1321	2.13	5.37	3.64 ± 0.36	2.83 ± 0.35
^{238}U	1625	2.50	5.21	3.15 ± 0.27	3.33 ± 0.33
^{237}Np	1535	2.20	4.54	3.56 ± 0.34	3.40 ± 0.25
^{239}Pu	2019	2.45	5.33	2.67 ± 0.12	4.11 ± 0.16
^{241}Am	1880	2.24	5.40	2.69 ± 0.31	4.13 ± 0.11

energy of the first nonevaporated neutron. However, as was discussed in Ref. [14], the latter value may be underestimated, hence leading to an overestimation of $\nu^{\rm post}$. A more accurate account of the neutrons emitted from the primary FFs could be provided by a full evaporation calculation for each primary FF produced at scission with an appropriate evaporation code. The total ν values are improved with respect to the default values (see Table 3 of [14]). Finally, the $\sigma_f^{\rm tot}$ obtained from Fit 1 also give a better account of the experimental fission cross sections. Similar results are obtained at $E_p = 62.9$ MeV. In this case, M_2 needs to be increased from 0.8 to 1.5, 2, and 3 to enhance $\sigma_f^{\rm tot}$ and $\nu^{\rm pre}$ for all the actinide targets except for ^{237}Np. In the latter case, M_2 has to be reduced (by 50%) just as for $E_p = 26.5$ MeV. A further readjustment of $K_{\rm rot}^{\rm const}$ for some of the individual FS is required and, in most cases, $K_{\rm rot}^{\rm const}$ is reduced for the most symmetric FS and increased for more asymmetric ones, with the exception of ^{232}Th. In spite of the various improvements observed at 62.9-MeV proton energy, describing the distinct symmetric peaks along with the pronounced asymmetric shoulders of all the experimental mass distributions proves to be a difficult task. What further complicates it is the fact that the calculated FF mass distributions contributing to symmetric partitions are generally broader than the experimentally observed symmetric peaks. In fact, they are as broad as the calculated asymmetric contributions. It is therefore not clear how it is possible to obtain FF mass distributions with the narrow symmetric peaks in agreement with experiment by solely modifying the relative contributions of the individual FS. We note that, in the fitting procedure described in this section, we prefer to use the maximum or minimum allowed values of $K_{\rm rot}^{\rm const}$ to obtain the desired agreement with data rather than use unreasonable values of B_f.

In spite of the significant improvements mentioned above, there are still some features of the experimental mass distributions that cannot be reproduced for any of the actinide targets. The calculated mass distributions are systematically

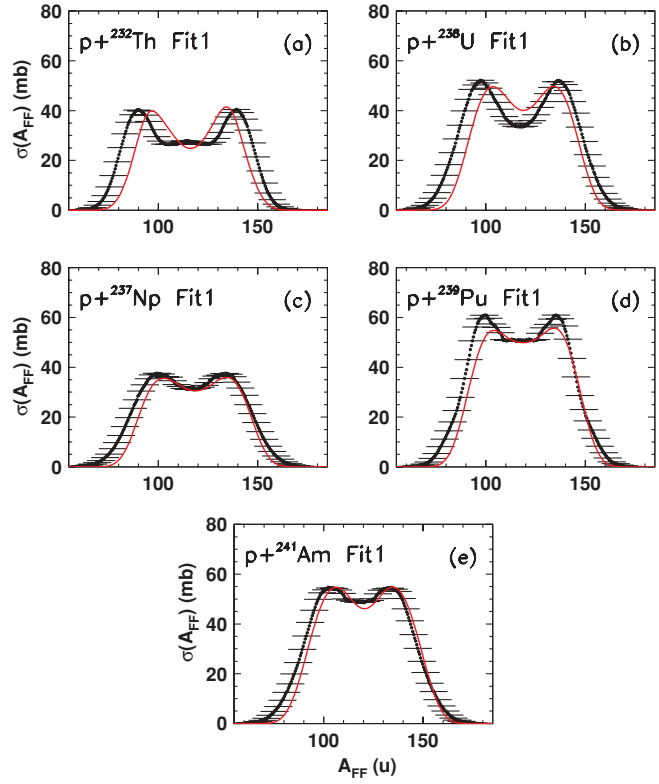

FIG. 11. (Color online) Total mass distributions $\sigma(A_{\rm FF})$ of fission fragments for proton-induced fission on ^{232}Th, ^{238}U, ^{237}Np, ^{239}Pu, and ^{241}Am target nuclei measured at incident proton energy 26.5 MeV [14] (black symbols). Also plotted are the calculated mass distributions produced with TALYS [3] using the modified values of M_2, B_f, and $K_{\rm rot}^{\rm const}$ (Fit 1) from Table II (red solid line).

shifted toward the heaviest FF with respect to the lighter ones and are always much narrower than the measured ones. The former effect could be explained by the different measured and calculated pre-scission neutron multiplicities that lead to different values of the mass at the scission point ($A_{\rm SCI}$) and hence to different values of the centroid ($A_{\rm SCI}/2$) of the FF mass distribution. In addition, we should also consider the fact that the experimental mass distributions suffer from some non-negligible experimental uncertainties as can be seen in Figs. 1, 2, 11, and 12. The latter uncertainties have been determined by taking into account effects such as the energy loss of the FF in the target, the straggling effects in energy and angle and, finally, the approximations involved in extracting the FF mass from the detection angles and the relative velocities instead of measuring the kinetic energies [14]. In plotting the experimental error bars in all the figures herein, it is assumed that these experimental uncertainties are equal to those of the symmetric mass splitting. From the above figures, one can see that the calculated FF mass distributions, although narrow, are marginally within the experimental uncertainties. Undoubtedly, the most outstanding problem remains the shape of the mass distribution of ^{232}Th at both incident energies. The symmetric peak, while less evident at 26.5 MeV, is rather pronounced at 62.9 MeV and cannot be described by the improved calculations (Fit 1). A similar softer

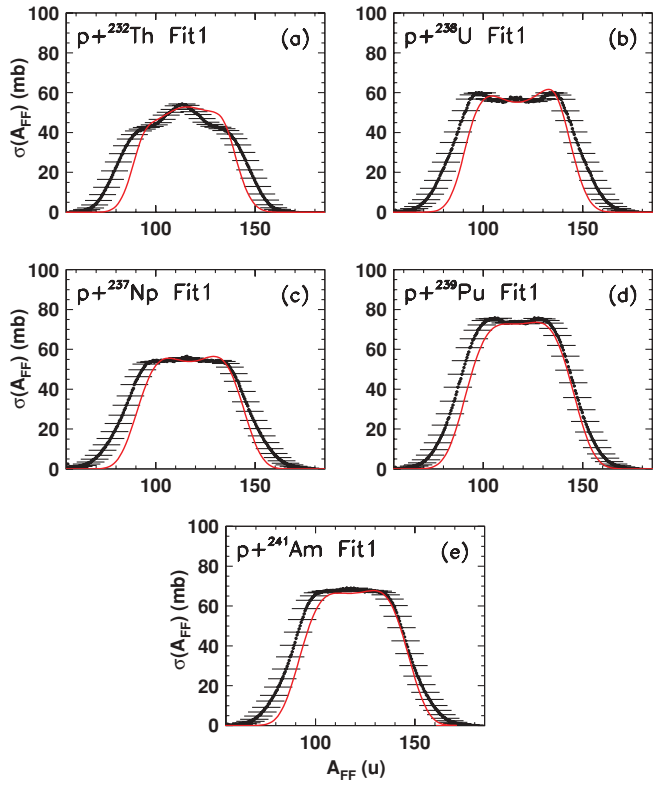

FIG. 12. (Color online) Same as Fig. 11 but for proton incident energy 62.9 MeV.

symmetric peak is also present in the measured distributions of the other actinide targets, and cannot be reproduced by the adjusted distributions either. In the following section we shall show that these features are strongly related to the fission modes of the MM-RNRM [4] and their respective weighting factors $W_{\rm FM}$.

B. Fission Modes

According to the MM-RNRM [4], the three fission modes, SL, STI and STII, give rise to rather different pre-scission shapes and, consequently, different FF mass distributions. The SL mode is related to a superlong shape of the FS and leads to a completely symmetric peak, STI is connected to an asymmetric and "normal" length shape and thus gives an asymmetric mass distribution (a component around $A \approx 135$), while STII corresponds to an even more asymmetric shape leading to even more asymmetric mass distributions than STI ($A \approx 142$). There is no precise method to calculate the weights $W_{\rm FM}$ of each FM other than by using the transmission coefficients $T_{f,\rm FM}$ through the barriers along the corresponding fission path or by adjusting them to experimental data. The latter approach, while practicable at low energies, becomes rather complicated and thus unfeasible at higher incident energies where several FS contribute to the fission process. In TALYS [3], the latter weights $W_{\rm FM}$ are calculated by taking into account the Hill-Wheeler transmission coefficients $T_{f,\rm FM}$ through the single-, double-, or triple-humped barriers along the corresponding fission path.

In this section, we shall modify the relative contributions of the FMs for all the contributing FS with the aim to investigate the sensitivity of the calculated FF mass distributions to the weights $W_{\rm FM}$ and ultimately to get a better description of the shapes of the experimental FF mass distributions. For this purpose, we start from the default parameters of TALYS and discard any adjustments performed in Fit 1 of the previous section. The fitting procedure is applied to ^{232}Th only since, in this particular case, we observe the most severe discrepancies between theory and experiment, as shown in the previous section. As we are interested in the shapes of the distributions only, the calculated FF mass distributions are normalized to the experimental ones in the following fitting procedure.

The weights $W_{\rm FM}(c)$ of the fission modes depend on the fission barriers along the path of the fission mode FM. They also vary with excitation energy since the implementation of the MM-RNRM in TALYS also includes T dependence. Modifying the contributions $W_{\rm FM}(c)$ for each FS obviously requires changing the parameters of the models that are used to determine the PES and fission barriers in the MM-RNRM. This is well beyond the scope of this article; however, in order to gain some insight into the FMs that give the correct shape of the mass distributions, we introduce empirical normalization coefficients $R_{\rm FM}$ for each FM [i.e., $W_{\rm FM}(c) = R_{\rm FM} W_{\rm FM}(c)$]. $R_{\rm FM}$ are identical for all FS and remain constant with excitation energy $E^{\star}_{\rm FS}$. From the comparisons in Figs. 1 and 2, one can see that the calculated FF mass distributions are too asymmetric with respect to the data. In this fitting procedure (Fit 2), we try to improve the calculations by eliminating one of the asymmetric FMs completely. We hereby take two separate extreme cases, one with $R_{\rm STII} = 0$, and the other with $R_{\rm STI} = 0$. The remaining two normalization coefficients in each case are adjusted to give the best description of the experimental FF mass distributions. The resulting FF mass distributions are shown in Fig. 13 for the ^{232}Th target nucleus at the two proton bombarding energies. The (red) solid curve was obtained with $R_{\rm SL} = 65$, $R_{\rm STI} = 35$, and $R_{\rm STII} = 0$, for both incident energies, while the (blue) dashed curve was obtained with $R_{\rm SL} = 20$, $R_{\rm STI} = 0$, and $R_{\rm STII} = 80$, again for both incident energies. One can observe an impressive improvement in the shapes of the mass distributions obtained in both extreme cases. In particular, the symmetric peak observed in the experimental data at both incident energies is nicely reproduced in the case of $R_{\rm STII} = 0$. However, the resulting mass distributions are still much narrower than the data, which is expected since the component that produces FF around $A \approx 142$ is missing. The mass distributions obtained with $R_{\rm STI} = 0$, on the other hand, are significantly broader than the data for 26.5-MeV incident proton energy, whereas for 62.9-MeV proton energy they are in good agreement with the experimental data. In the latter case, the asymmetric shoulders are not that well reproduced due to the missing STI component (around $A \approx 135$).

The results of Fit 2 show that the shapes of the FF mass distributions are very sensitive to the relative contributions of the FMs of the MM-RNRM [2,4]. The resulting values of $R_{\rm FM}$ are entirely empirical and may not be physical, as all three FMs are expected to contribute to fission of actinides.

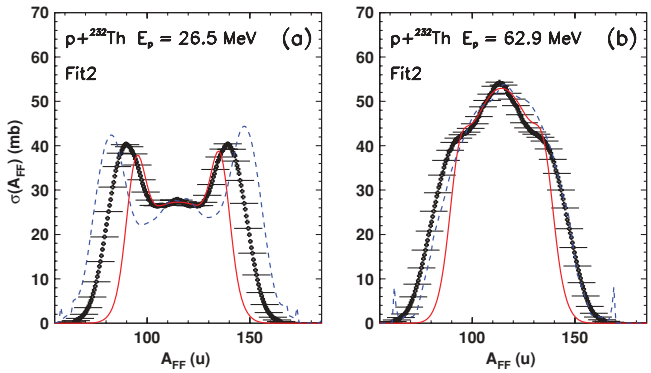

FIG. 13. (Color online) (a) Normalized mass distributions $\sigma(A_{\rm FF})$ of fission fragments for proton-induced fission on ^{232}Th target measured at incident proton energies of 26.5 MeV [14] (black symbols) compared with the mass distributions calculated with modified weights $R_{\rm FM}W_{\rm FM}$ (Fit 2) (red solid and blue dashed lines, see text for details). (b) Same as in (a) but for an incident proton energy of 62.9 MeV.

However, they do indicate that the contributions of the SL or STII modes need to be enhanced with respect to STI in order to obtain simultaneously the broader FF mass distributions observed in the experimental data and a nice reproduction of the pronounced symmetric peak. It is likely that this desired enhancement could be achieved by using a more suitable microscopic model for the description of the PES and triple-humped fission barriers of the ^{232}Th target nucleus in the MM-RNRM implemented in TALYS [2]. More theoretical work is needed in this direction.

III. CONCLUSIONS

Fission properties including FF mass distributions $\sigma_f^{\rm tot}$ and pre- and post-scission neutron multiplicities $\nu^{\rm pre}$ and $\nu^{\rm post}$, respectively, measured for proton-induced fission on ^{232}Th, ^{237}Np, ^{238}U, ^{239}Pu, and ^{241}Am target nuclei, at proton energies of 26.5 MeV and 62.9 MeV [14], have been compared with the predictions of the nuclear reaction code TALYS [3]. The code couples the pre-equilibrium and statistical models with the MM-RNRM [2,4] and thus provides total fission cross sections, FF mass and charge distributions, and neutron multiplicities for a wide range of nuclei and energies. Calculations have been performed with different sets of fission barriers (Maslov [17], RFRM [18], RLDM [19]) available in the code. The results overall underestimate the magnitude of the FF mass distributions and $\sigma_f^{\rm tot}$ and fail to give the correct contributions of symmetric and asymmetric mass partitions. The predictions also tend to overestimate $\nu^{\rm pre}$ at $E_p = 26.5$ MeV and underestimate it at $E_p = 62.9$ MeV. A limitation in the calculations of the FF mass distributions should be noted; namely, that the different sets of fission barriers available in TALYS can, so far, only be used in the fission cross-section calculations within the statistical model. On the other hand, the mass partitions $[(Y(A_{\rm FF};c)]$ determined by the MM-RNRM are based solely on the barriers obtained from the LDM plus shell corrections inherent in the version of the MM-RNRM of Ref. [2].

The calculations were improved by modifying (i) the relative contribution of PE emission and CN decay by adjusting the magnitude of the exciton-model interaction [15] and (ii) the contributions of the individual FS through their corresponding cross sections σ_f (Fit 1). The adjusted values of M_2, $K_{\rm rot}^{\rm const}$ and B_f give a better description of the magnitude of the FF mass yields $\sigma_f^{\rm tot}$ and $\nu^{\rm pre}$ at both proton energies and for all the actinide targets. The relative contribution of symmetric and asymmetric fission partitions is improved considerably with respect to the default results. However, in almost all of the cases, the adjustable parameter $K_{\rm rot}^{\rm const}$ had to be set to its extreme values and, in some cases, B_f had to be reduced to unreasonably low values in order to obtain the desired result.

The improvements (Fit 1) mentioned above were not able to describe the symmetric peak that is observed in all the mass distributions and is particularly pronounced for the ^{232}Th target. The features of the FF mass distributions also depend on the relative contributions of the FMs which are determined within the MM-RNRM [2,4]. The original mixed contribution of all three FMs, namely SL, STI, and STII is not suitable to describe proton-induced fission of ^{232}Th in particular, at the energies of 26.5 MeV and 62.9 MeV. The relative weights of the three FMs, expressed by $R_{\rm FM}W_{\rm FM}$, were subsequently adjusted to the shapes of the mass distributions of a ^{232}Th target at both proton energies. The results show that setting $R_{\rm STII} = 0$ leads to a better description of the symmetric peaks but gives very narrow widths, while with $R_{\rm STI} = 0$ the widths are significantly broader, in agreement with experiment.

The above-mentioned adjustments (Fit 1 and Fit 2) are purely empirical and the obtained values of the parameters should not be taken at face value without further confirmation from comparisons with other independent data. Nevertheless, the trends observed in the adjusted parameters (i.e., the need to use extreme values of $K_{\rm rot}^{\rm const}$ in Fit 1 for all five actinide targets ^{232}Th, ^{237}Np, ^{238}U, ^{239}Pu, and ^{241}Am, and $R_{\rm STI/STII} = 0$ in Fit 2 for ^{232}Th) shows that certain properties of the actinide nuclei are inadequately described by both the statistical model and the MM-RNRM as implemented in TALYS [3]. Further theoretical work is required to investigate the nuclear models and parameters relevant for fission as well as the coupling of the statistical model with MM-RNRM in TALYS. With regards to the latter coupling of the two different models, in particular, it would be worth exploring how this coupling could be improved in terms of using consistent parameters derived from one and the same microscopic theory using a suitable effective interaction. For this purpose, more experimental data on proton- and neutron-induced fission reactions over a wide range of energies and masses would also be useful.

ACKNOWLEDGMENTS

One of us (P.D.) would like to acknowledge the catholic University of Louvain for its hospitality during her multiple stays in Belgium.

[1] G. Aliberti, G. Palmiotti, M. Salvatores, and C. G. Stenberg, Nucl. Sci. Eng. **146**, 13 (2004).
[2] M. C. Duijvestijn, A. J. Koning, and F.-J. Hambsch, Phys. Rev. C **64**, 014607 (2001).
[3] A. J. Koning, S. Hilaire, and M. C. Duijvestijn, in *Proceedings of the International Conference on Nuclear Data for Science and Technology, Santa Fe, New Mexico, 2004*, edited by R. Haight *et al.* AIP Conf. Proc. No. 769 (New York, USA, 2005), pp. 1154–1159.
[4] U. Brosa, S. Grossmann, and A. Mueller, Phys. Rep. **197**, 167 (1990).
[5] V. P. Eismont, in *Final Project Technical Report ISTC* 540-97 (1997).
[6] V. P. Eismont *et al.*, in *Proceedings of 3rd International Conference on Accelerator Driven Transmutation Technologies and Applications, Praha (Pruhonice), Czech Republic*, 7–11 June 1999.
[7] V. P. Eismont *et al.*, in *TSL Progress Report 1998–1999*, Vol. 38, edited by. A. Ingemarsson (Uppsala University, 2000).
[8] I. Ryzhov *et al.*, Nucl. Instrum. Methods Phys. Res. A **562**, 439 (2006); (private communication, 2009).
[9] V. P. Eismont *et al.*, in *Proceedings of the International Conference on Accelerator Driven Transmutation Technologies, Kalmar, Sweden*, 3–7 June 1996, edited by H. Condo, p. 592.
[10] V. P. Eismont *et al.*, in *Proceedings of the International Conference on Future Nuclear Systems, GLOBAL 97, 5–10 October 1997, Yokohama, Japan*, p. 1365.
[11] M. C. Duijvestijn, A. J. Koning, J. P. M. Beijers, A. Ferrari, M. Gastal, J. vanKlinken, and R. W. Ostendorf, Phys. Rev. C **59**, 776 (1999).
[12] T. Ohtsuki *et al.*, Phys. Rev. C **44**, 1405 (1991).
[13] V. A. Rubchenya *et al.*, Nucl. Instrum. Methods Phys. Res. A **463**, 653 (2001).
[14] S. Isaev, R. Prieels, T. Keutgen, J. V. Mol, Y. El Masri, and P. Demetriou, Nucl. Phys. A **809**, 1 (2008).
[15] A. J. Koning and M. C. Duijvestijn, Nucl. Phys. A **744**, 15 (2004).
[16] E. S. Soukhovitskii, S. Chiba, J. Y. Lee, O. Iwamoto, and T. Fukahori, J. Phys. G: Nucl. Part. Phys. **30**, 905 (2004).
[17] R. Capote *et al.*, Nucl. Data Sheets **110**, 3107 (2009). [http://www.nds-iaea.org/RIPL-2/]
[18] A.J. Sierk, Phys. Rev. C **33**, 2039 (1986).
[19] S. Cohen, F. Plasil, and W. J. Swiatecki, Ann. Phys. **82**, 557 (1974).
[20] J. F. Croall and J. G. Cuninghame, Nucl. Phys. A **125**, 402 (1969).